# C–C $\sigma$ complexes of rhodium

**Simon K. Brayshaw*, Emma L. Sceats†, Jennifer C. Green†§, and Andrew S. Weller*§**

*Department of Chemistry, University of Bath, Bath BA2 7AY, United Kingdom; and †Inorganic Chemistry Laboratory, South Parks Road, Oxford OX1 3QR, United Kingdom

Edited by Jay A. Labinger, California Institute of Technology, Pasadena, CA, and accepted by the Editorial Board February 2, 2007 (received for review November 6, 2006)

**In this article, the complexes [Rh(Binor-S′)($PR_3$)][$BAr^F_4$] (R = $^i$Pr, Cy, $C_5H_9$) are described. A combination of x-ray crystallography, NMR spectroscopy, density functional theory, and ''atoms in molecules'' calculations unequivocally demonstrates that the complexes contain rare examples of metal···C–C agostic interactions. Moreover, they are fluxional on the NMR time scale, undergoing rapid and reversible C–C activation. Kinetic data and calculations point to a bismetallacyclobutane, Rh(V), intermediate.**

C–C activation | density functional theory

The activation of carbon–carbon (C–C) single bonds by transition metals is an area of chemistry that continues to attract considerable interest (1–6). The elucidation of the mechanism of C–C activation and the isolation of intermediates in such processes remain a significant challenge. In spite of this challenge, the use of C–C activation as a practical method for the construction of organic molecules is becoming more common, and even catalytic routes now are synthetically viable (3, 7, 8). This finding follows longer-established C–H activation methodologies, which now are commonplace in transition metal catalyzed organic synthesis (9, 10). Although thermodynamically C–C activation can be favored over C–H activation when relative C–C, M–C, C–H, and M–H bonds strengths are considered (11), kinetically C–C activation is disfavored because of the relative inaccessibility of the directional C–C bond compared with C–H (12, 13). For this reason, C–C activation by transition metal complexes generally involves substrates that either are intrinsically strained [e.g., unstrained C–C bonds E(C–C) $\approx$90 kcal·mol$^{-1}$, compare with biphenylenes, E(C–C) 65.4 kcal·mol$^{-1}$ or cyclopropanes, E(C–C) 61 kcal·mol$^{-1}$] or the C–C bond in question is held in close proximity to the metal center (2, 7, 14–16).

Parallels between C–C, C–H, and more generally X–H (X = main group atom) activation extends to mechanistic considerations (10, 17, 18). Although there are a number of mechanisms for C–H activation at a metal center (C–H oxidative addition, electrophilic activation, and $\sigma$-bond metathesis) (19), they proceed through intermediates in which the C–H bond uses its $\sigma$-bonding pair to coordinate to the metal center (17, 20–22). Similarly, C–C activation often is proposed to proceed through C–C $\sigma$ complexes (Scheme 1). For example, Zeise's dimer, [$PtCl_2(\eta^2$-$C_2H_4)]_2$, is proposed to react with cyclopropane via a C–C $\sigma$ intermediate (6); both Bergman and colleagues (23) and Jones and colleagues (24) present convincing mechanistic data for such intermediates in the rearrangement of rhodium cyclopropyl hydrido complexes to metallacyclobutanes. ''Edge-metallated'' cyclopropane complexes have been suggested as intermediates in olefin cyclopropanation reactions mediated by palladium dicarboxylates (25), and calculations on the interaction of the C–C bond in ethane with Pt in the model complex [$PtMe(PH_3)_2(\eta^2$-$C_2H_6)]^+$ also suggest a $\sigma$ intermediate (26).

Well characterized examples of M···C–C $\sigma$ interactions are extremely rare [one example of an analogous $\eta^2$-Si–Si sigma bond recently has been reported (27, 28)]. All examples are intramolecular (i.e., agostic) rather than intermolecular. von Ragué Schleyer and colleagues (29) have reported the synthesis, solid-state structure, and accompanying theoretical analysis of a lithiated cylcopropyl alcohol that shows the $Li^+$ cation to straddle the C–C edge in cyclopropane (Scheme 2, complex **I**). A transition metal complex with a C–C···M agostic bond characterized both crystallographically and in solution was reported by Ernst and colleagues (30, 31) (Scheme 2, complex **II**). On the basis of very short Ti···C distances to saturated carbon atoms, lower than expected $^{13}C$–$^{13}C$ coupling constants, and a theoretical natural bond order (NBO) analysis, agostic C–C···Ti interactions were proposed, although the presence of these have been questioned since (32). Milstein and colleagues have characterized a number of PCP- and PCN-type rhodium pincer complexes (e.g., Scheme 2, complexes **III**) in solution that are proposed to have agostic M···C–C interactions on the basis of NMR data and a solid-state structure that shows a closer than van der Waals separation between Rh and C(2, 33–35). Etienne and colleagues have described the niobium cyclopropyl complex **IV** that shows a close Nb···C–C contact and lengthening of the C–C distance in the cyclopropyl group consistent with an agostic C–C···Nb interaction (36, 37). An early report of an agostic C–C complex recently has been reassessed by Maseras and Crabtree (38) as one that has a close nonbonding contact with a C–C bond and not an agostic species. Agostic M···C–C interactions also have been proposed to be present in metallacyclobutane complexes (19, 31, 39). Examples of agostic M···C–C complexes that then proceed on to C–C cleavage to form a metal alkyl species, as far as we are aware, have not been directly observed even though they are strongly implicated in such transformations. Interestingly, the reverse is known. Milstein and colleagues have reported that Rh(III) methyl PCP-pincer complexes undergo methyl migration to form a Rh···C–C agostic species (33, 35, 40). In contrast, mechanistic studies into C–C activation in a neutral PCN-pincer rhodium complex identify a spectroscopically characterized intermediate at low temperature that does not appear to have a Rh···C–C interaction (41).

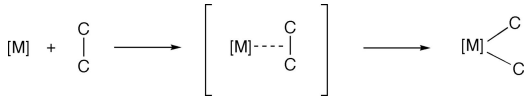


Scheme 1.

The lack of well characterized examples of species with M···C–C interactions is in contrast with M···HC agostic $\sigma$ complexes that are well established (42, 43), some of which go on to C–H activate (44).

Author contributions: J.C.G. and A.S.W. designed research; S.K.B. and E.L.S. performed research; S.K.B., E.L.S., J.C.G., and A.S.W. analyzed data; and E.L.S., J.C.G., and A.S.W. wrote the paper.

The authors declare no conflict of interest.

This article is a PNAS Direct Submission. J.A.L. is a guest editor invited by the Editorial Board.

Abbreviations: DFT, density functional theory; AIM, ''atoms in molecules''; nbd, norbornadiene; BCP, bond critical point; RCP, ring critical point.

Data deposition: The crystallographic data have been deposited in the Cambridge Structural Database, Cambridge Crystallographic Data Centre, Cambridge CB2 1EZ, United Kingdom (CSD reference nos. 280042, 632492, and 632493).

§To whom correspondence may be addressed. E-mail: a.s.weller@bath.ac.uk or jennifer.green@chemistry.oxford.ac.uk.

This article contains supporting information online at www.pnas.org/cgi/content/full/0609824104/DC1.

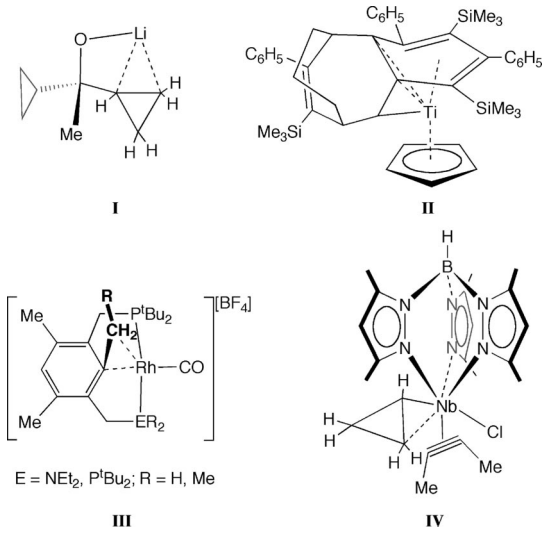


Scheme 2.

Further examples of genuine, fully characterized examples of M···C–C $\sigma$ interactions are of clear importance regarding the fundamental study of C–C activation processes, the development of transition metal catalyzed C–C activation, and $\sigma$ complexes in general. We report here in full the synthesis of a set of complexes that show such M···C–C agostic interactions that also undergo facile and reversible C–C activation in solution on the NMR time scale. These complexes have been characterized by solid-state solution, and theoretical [density functional theory (DFT) combined with an "atoms in molecules" (AIM) analysis] studies. We also present calculations on a model complex that supports our analysis of the fluxional mechanism. Aspects of this work have been communicated previously (45).

## Results and Discussion

**Synthesis and Solid-State Structures.** Addition of excess norbornadiene (nbd) to fluorobenzene solutions of $Rh(PR_3)(nbd)Cl$, where R = isopropyl ($^i$Pr), cyclohexyl (Cy), and cyclopentyl (Cyp), in the presence of the halide abstracting agent $Na[BAr^F_4]$ ($BAr^F_4$ = $B\{C_6H_3(CF_3)_2\}_4$) results in the formation of the complexes $[Rh(PR_3)(Binor\text{-}S')][BAr^F_4]$ **1** R = $^i$Pr, **2** R = Cy, and **3** R = Cyp (Scheme 3). These complexes are purified by crystallization as air-sensitive materials in good isolated yield (53–82% based on rhodium). Also formed in the reaction are the products of nbd dimerization, principally Binor-S, which arises from a 4 + 4 cycloaddition of the diene. The dimerization of nbd first was reported by Schrock and Osborn using $[Rh(nbd)_2][PF_6]$ and $PPh_3$ (46), although little comment was made on the structure of the active species. Indeed, complexes **1**–**3** are isolated resting states of this catalytic system, as addition of further nbd results in the production of more Binor-S. Complexes **1**–**3** are isolated at the end of the catalytic reaction when the diene has been consumed. An alternative route to these complexes is the addition of one equivalent of phosphine to $[Rh(nbd)_2][BAr^F_4]$. This route affords the complexes in good yield without the formation of excess Binor-S. All of the complexes are air-sensitive. They decompose in $CD_2Cl_2$ ($t_{1/2}$ = 16 h) but are more stable in fluorobenzene solution (for several days) under argon.

The solid-state structure of complexes **1**, **2**, and **3** are shown in Fig. 1. All three complexes show very similar structural motifs in the solid state, and selected bond lengths and angles are collected in Table 1. Supporting information (SI) Table 2 provides a fuller listing of the structural metrics.

All three structures show a cationic rhodium complex coordinated with one alkyl phosphine ligand and a saturated alkyl ligand derived from Binor-S (47) (referred to as Binor-S′) by oxidative addition across one of the cyclopropane rings to form a metallacyclobutane. They adopt approximate $C_s$ symmetry in the solid state. The geometry of the Binor-S′ ligand means that the remaining cyclopropane ring [C(21)/(25)/(26)] is orientated so that there is a close approach of the C(21)–C(25) single bond to the metal center. The two Rh–C bonds in the metallacyclobutane ring (Rh–C11 and Rh–C15) have distances that are similar but a little shorter than in the rhodium(III) metallacyclobutane complex $Rh(\eta^5\text{-}C_5Me_5)(PMe_3)(CH_2)_3$ (23). The coordination sphere of rhodium is completed by γ-agostic C–H bonds. For **1**, there are two closer CH···Rh distances [2.52 (4) and 2.77 (3) Å] from the same methyl group, whereas for **2** and **3** there are two separate methylene interactions of comparable distances. All of these distances (lying in the range H···Rh 2.52–2.8 Å; Table 1) would be considered to be long for M···HC agostic interactions (48) and suggest that they are, at best, weak. With the overall positive charge and two alkyl Rh–C bonds, the formal oxidation state is described as Rh(III).

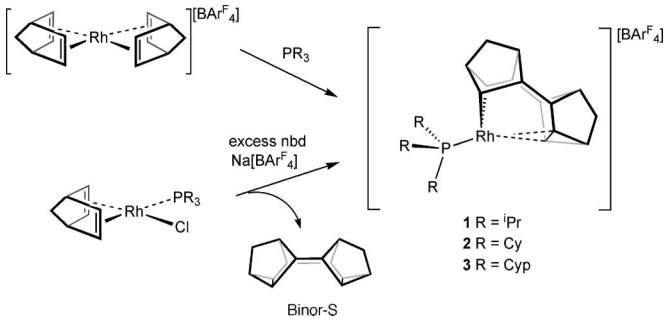


Scheme 3.

Attention now turns to the close distance between Rh and the cyclopropyl fragment defined by C21/C25/C26. For all of the compounds **1**–**3**, the two Rh···C distances lie between 2.349 (3) and 2.387 (2) Å (Table 1), with **2** showing the (marginally) longer distances. These distances lie well within the van der Walls radii of Rh and C(≈3.3 Å) and are only ≈0.3 Å longer than expected for a Rh–C single bond. On comparison with other transition metal systems that show close C–C···metal distances in the solid state, they also are short, even taking into account the disparate van der Waals radii of each metal [e.g., Ti···C: 2.579 (7) and 2.293 (7) Å (ref. 30; Scheme 2, complex **II**); Rh···C: 2.817 Å (ref. 33; Scheme 2, complex **III**); and Nb···C: 3.045 (3) Å (ref. 36; Scheme 2, complex **IV**)]. The hydrogen atoms on the cyclopropyl ring C(21)/C(25)/C(26) also lie relatively close to the Rh center [e.g., Rh–H (25) 2.30 (5) Å and Rh–H (21) 2.32 (3) Å in **1**] and certainly are within the distance associated with second-row agostic M···HC bonds (48). The question that arises is as to the nature of this close approach of the cyclopropyl group. Is it a C–C agostic or C–H agostic interaction, a combination of both, or neither and just a close approach of a saturated C–C bond with no significant bonding to the metal (32, 38)? We answer this question through the combination of structural reporters, spectroscopic (NMR) evidence, and DFT calculations.

Within the limits of the x-ray diffraction experiment, the C–H bonds associated with C(21) and C(25) are not significantly lengthened [average 0.97 (3) Å]. Agostic C–H interactions to late transition metals usually result in a lengthening of the C–H bond by ≈10% (49). In contrast, the C(21)–C(25) bond in the Binor-S′ fragment [average 1.606 (4) Å] is lengthened by 7–8% (0.11–0.12 Å) compared with the equivalent distances in the two other crystallographically characterized compounds based on Binor-S (SI Fig. 4) (47, 50). The other two C–C distances in the cyclopropyl ring are not lengthened. A similar, but smaller, lengthening of the C–C distance of 0.049 Å (≈3%) was noted in

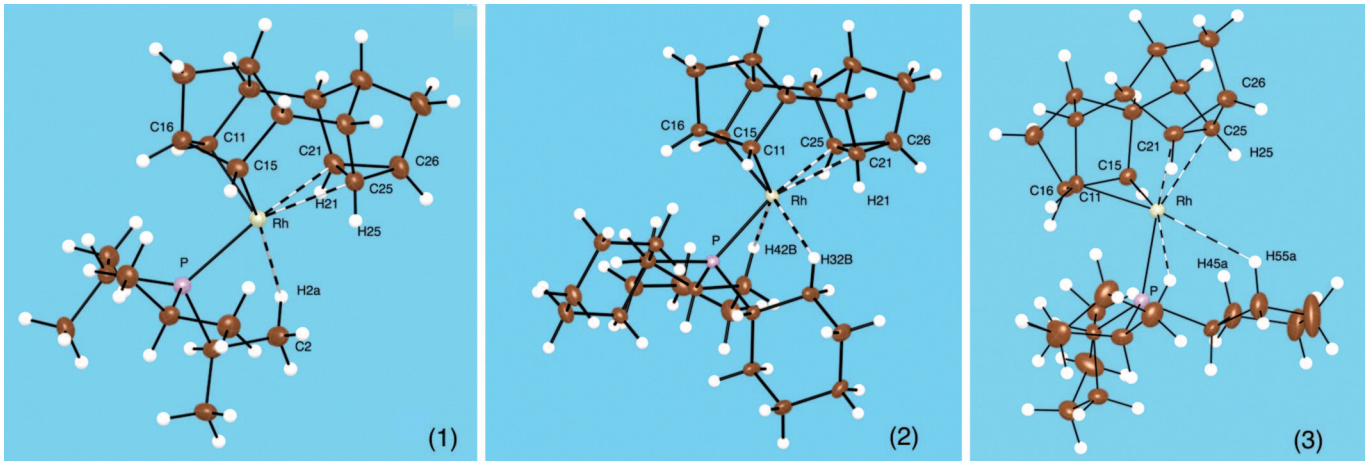


**Fig. 1.** Solid-state structure of complexes **1**, **2**, and **3**, with only the cation shown. Thermal ellipsoids are shown at the 50% probability level. Dashed lines indicate the agostic C–C···Rh and agostic C–H···Rh interactions.

compound **IV** (Scheme 2) and suggested to be diagnostic of a C–C agostic bond, consistent with donation of $\sigma$ electron density to the metal. Calculations on C–C activation of cyclopropane by rhodium and iridium complexes indicate transition states stabilized by a C–C agostic interaction that have lengthened C–C bonds (51), whereas "edge-bridged" cyclopropane palladium dicarboxylates are suggested to be intermediates in cyclopropanation reactions and calculated to show a lengthening of the coordinated C–C single bond between 5% and 13% (25). Together, these observations are consistent with relatively tight C–C···Rh agostic interactions in complexes **1**–**3**. As we will demonstrate later, the structural features of the Binor-S-derived complexes (lengthened C–C distance, unchanged C–H distances) also are reflected accurately in DFT calculations. Finally, the phosphine ligand is orientated trans to the agostic Rh···C–C bond with the two weak agostic C–H interactions trans to the Rh·alkyl bonds. This arrangement is as expected on the basis of trans-influence arguments (52).

NMR data also help elucidate the nature of the Rh···C–C interaction. All three complexes show very similar solution NMR data for the Binor-S′ fragment, and we therefore concentrate on complex **1** for brevity. Full spectroscopic data can be found in the SI Table 3. Unlike the solid-state structure, at 298 K in $CD_2Cl_2$ solutions, the Binor-S′ ligand has time-averaged $C_{2v}$ symmetry, just as in free Binor-S, which is shown by only five and four[¶] resonances being observed in the $^1$H NMR and $^{13}C\{^1H\}$ NMR spectra at room temperature for the Binor-S′ ligand, although if the solid-state structures were retained in solution at 298 K, 10 resonances would be expected for both ($C_s$ symmetry). This finding must mean that there is a dynamic process occurring that makes equivalent C(11)/(15) (metallacyclobutane) and C(21)/(25) (cyclopropane). By using $^1$H–$^1$H and $^{13}$C–$^1$H correlation experiments, the signal for C(11)/(15)/(21)/(25) at room temperature is identified in the $^{13}C\{^1H\}$ NMR spectrum at $\delta = 25.5$ and the associated hydrogen atoms at $\delta = 3.23$ in the $^1$H NMR spectrum. Coupling to $^{103}$Rh and $^{13}$P also is observed in the $^{13}C\{^1H\}$ NMR spectrum [dd $^1J$(RhC) 12.4 Hz, $^2J$(PC) 4.4 Hz].[‖] This finding shows that there must be a significant, time-averaged Rh···C interaction in solution at room temperature.

Progressive cooling slows this fluxional process so that at 200 K the expected 10 signals from the solid-state structure are observed (SI Fig. 5). In particular, the CH(11)/(15)/(21)/(25) signal now resolves into two pairs of resonances in both the $^1$H and $^{13}C\{^1H\}$ NMR spectra. These have been assigned by $^1$H–$^1$H and $^{13}$C–$^1$H correlation experiments as being the pairs CH(11)/(15) [$\delta(^{13}C)$ 25.30, $\delta(^1H)$ 3.41] and CH(21)/(25) [$\delta(^{13}C)$ 23.78, $\delta(^1H)$ 2.78]. The $^{13}$C chemical shifts for Rh–C(11)/C(15) are more downfield than expected for a Rh–metallacyclobutane [e.g., Rh($\eta^5$-$C_5Me_5$)($PMe_3$)($C_3H_6$) shows the $\alpha$-cyclobutane carbons at $\delta = -22.8$ ppm (23)], which we attribute to ring strain in the Binor-S′ fragment. At 200 K, the $J$(HC) coupling constant for CH(21)/(25) is 170 Hz in **1** (172 Hz in **2** and 171 Hz in **3**) as measured from fully coupled heteronuclear multiple quantum correlation (HMQC) experiments (SI Table 4). These are essentially the same as found in free Binor-S [$J$(HC) 174 Hz] and argue against agostic CH···Rh interactions because such interactions would result in a significantly decreased $J$(HC) coupling constant. In the $^{13}C\{^1H\}$ NMR spectrum, the peak assigned to C(11)/(15) at $\delta = 25.30$ also displays coupling to $^{103}$Rh [$J$(RhC) 22.1 Hz] as does C(21)/C(25) $\delta = 23.78$ [$J$(RhC) 9.2 Hz].[**] The smaller coupling constant to C(21)/C(25) is consistent with a weaker agostic interaction. However, its observation also shows that there must be a significant interaction with the $\{Rh(P^iPr_3)\}^+$ fragment. For each of the complexes, the $^{31}P\{^1H\}$ NMR spectrum shows a single resonance that is essentially invariant over the temperature range studied and retains a large $J$(RhP) coupling constant. Overall, the observations of (*i*) a close Rh···C(21)/(25) distance in the solid state, (*ii*) a concomitantly increased C–C bond length, and (*iii*) coupling between the $\{Rh(PR_3)\}^+$ fragment and C(21)/C(25) with no significant change in the $J$(CH) coupling constant at low temperature all are strongly supportive of an agostic Rh···CC interaction in both solution and the solid state.

**Reversible C–C Activation in Solution.** The fluxional process occurring in these complexes in solution is one that exchanges the metallacyclobutane and cyclopropane fragments, and we postulate that this occurs via a concerted or stepwise C–C oxidative addition/reductive elimination of the Binor-S fragment. This process retains the Rh–P bond, as large $J$(RhP) coupling is observed throughout the temperature range in the $^{31}P\{^1H\}$ NMR spectrum. The Binor-S′ fragment does not undergo exchange with free Binor-S in solution as shown by exchange spectroscopy (EXSY) experiments, demonstrating that it remains associated with the metal center

[¶]The signal due to C26/C16 was not observed in the $^{13}C\{^1H\}$ NMR spectrum at room temperature. The calculated coalescence temperature is ≈280 K, and as a result, the signal would be expected to be broad in the room temperature spectrum.

[‖]We cannot be certain of the order of these couplings and suggest that the larger coupling is due to $^1J$(RhC).

[**]We cannot rule out that this coupling is due to $^{31}$P rather than $^{103}$Rh, with $J$(RhC) ≈ 0 Hz. However, the same conclusions hold with regard to the interaction between C(21)/(26) and the $\{Rh(PR_3)\}^+$ fragment.

**Table 1. Selected bond lengths (Å) for complexes 1–3**

| Bond | 1 | 2 | 3 |
|---|---|---|---|
| Rh–C(21)/C(25) | 2.352(3)/2.369(3) | 2.387(2)/2.385(2) | 2.355(3)/2.349(3) |
| Rh–C(11)/Rh–C(15) | 2.032(3)/2.042(3) | 2.027(2)/2.025(2) | 2.034(2)/2.029(2) |
| Rh–$HC_{agostic}$ | 2.52(4), 2.77(3) | 2.61(3)/2.78(2) | 2.63(3)/2.72(3) |
| Rh–P | 2.2693(7) | 2.2621(4) | 2.2466(7) |
| C(11)···C(15) | 2.205(4) | 2.234(3) | 2.229(4) |
| C(21)–C(25) | 1.604(4) | 1.608(3) | 1.607(4) |
| C(21)–C(26) | 1.510(4) | 1.514(3) | 1.521(4) |
| C(26)–C(25) | 1.502(4) | 1.514(3) | 1.518(4) |

during the fluxional process. Simulation (53) of the experimental $^1$H NMR spectra of **1** over the temperature range 298 K to 200 K allows rate data to be extracted for the exchange process. An Eyring plot gives values of $\Delta H^{\ddagger} = 9.6 \pm 0.2$ kcal·mol$^{-1}$, $\Delta S^{\ddagger} = -4.5 \pm 1$ cal·mol$^{-1}$·K$^{-1}$, and $\Delta G^{\ddagger} = (298)\ 10.7 \pm 1$ kcal·mol$^{-1}$ in $CD_2Cl_2$. All three complexes show effectively identical activation energies for the fluxional process. They also show no dependence on solvent, as recording the variable temperature spectra in $C_6D_5CD_3$ or 1,2-difluorobenzene resulted in essentially no change in the coalescence temperature for **1**. This finding is consistent with a fluxional process that does not involve a solvent-coordinated species.

On the basis of these observations, two possible mechanisms are suggested for the fluxional process (Scheme 4). The first involves a Rh(III)/Rh(I)/Rh(III) pathway and a biscyclopropane intermediate (pathway A). The second involves a Rh(V) bismetallacyclobutane intermediate (pathway B). Rh(V) compounds, although not common, have been described (54–56). Both pathways are consistent with a small negative value for $\Delta S^{\ddagger}$ in as much as the transition state is ordered but does not require a significant amount of structural reorganization to achieve it. As we present later, calculations suggest that pathway B is preferred. Attempts to find intermediates or transition states on pathway A either gave those found for pathway B or reverted to the ground state, which is in contrast to the reactivity of **1** that behaves as if it were a latent Rh(I) fragment, e.g., reaction with CO results in $[Rh(P^iPr_3)(CO)_3][BAr^F_4]$ plus free Binor-S (45) and suggests that the mechanisms of fluxionality and reactivity do not proceed through common intermediates.

Comparisons with other C–C activation processes for which activation parameters are known show that for the Binor-S′ systems, C–C activation is more favorable. For example, Milstein and colleagues (41) have reported the single C–C activation step in neutral rhodium PCN-pincer complexes related to III, and Jones and colleagues (57) have reported the C–C activation of allyl cyanide on nickel phosphines. Both of these processes have activation energies that are higher than for **1** (17.2 and 22.7 kcal·mol$^{-1}$, respectively), consistent with a strained cyclopropane-like ligand facilitating C–C activation in **1**. However, they also have similar small, and negative, entropies for activation, as does **1**, consistent with a preorganized transition state.

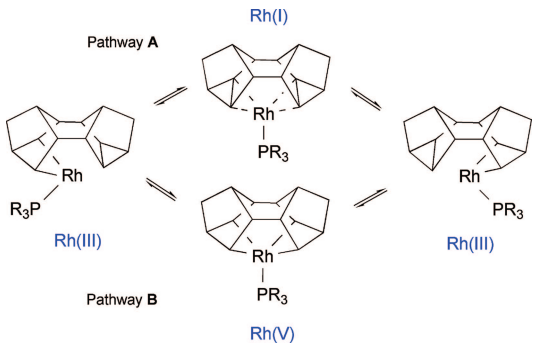


**Scheme 4.** Possible mechanistic pathways for the fluxional process in **1–3**.

**Electronic Structure.** DFT calculations have been used in conjunction with Bader's AIM approach (58, 59) to study the molecular and electronic structures of complexes **1** and **2**. Of special interest is the interaction between rhodium and the cyclopropyl fragment defined by C(21)/C(25)/C(26), which both solid-state and solution studies indicate to be an agostic Rh···C–C $\sigma$ interaction. Calculated geometric parameters for complexes **1** and **2** are listed in SI Table 5. In general, the calculated structures for these two complexes reproduce well the experimental solid-state structures. Importantly, parameters for the two Rh–C bonds in the metallacyclobutane ring [Rh–C(11)/(15), **1** 2.056/2.056 Å, **2** 2.021/2.019 Å] and those for the Rh···C–C $\sigma$ interaction [C(21)–C(25), **1** 1.614 Å, **2** 1.607 Å; Rh–C(21)/(25), **1** 2.418/2.416 Å, **2** 2.328/2.321 Å] are in excellent agreement with those obtained from x-ray diffraction measurements (Table 1). Furthermore, the C–H bonds associated with C(21) and C(25) are not significantly lengthened (calculated average C–H bond length is 1.104 Å), especially when compared with the $\gamma$-agostic C–H bonds that complete the coordination sphere of rhodium [e.g., C(2)–H(2a) 1.12 Å in **1**].

The AIM approach, which uses a topological analysis of the electron distribution to characterize bonding interactions, has been used to study these cationic rhodium species. A brief communication of the analysis for **1** has been reported previously (57). Selected bond critical points (BCPs) and ring critical points (RCPs) for complexes **1** and **2** are listed in SI Table 5. In general, characteristics of the critical points located in an AIM analysis of **2** are very similar to those determined for **1**, and we therefore concentrate on **1** in the interests of brevity.

AIM analysis of **1** shows the expected (3, −1) BCP between C(25)–C(21) (BCP 1) and BCPs on the bond paths linking Rh–C(15) (BCP 14) and Rh–C(11) (BCP 15), i.e., the Rh–C $\sigma$ bonds of the metallacyclobutane ring. The existence of a Rh···C–C agostic interaction was confirmed by the presence of BCPs between Rh–C(25) (BCP 8) and Rh–C(21) (BCP 9) and by the interatomic surface, which bisects the bond paths linking rhodium and C(21)/C(25). A description of **1**, including an agostic Rh–HC interaction rather than a Rh···C–C $\sigma$ interaction, was ruled out on the basis of the absence of BCPs between Rh and H(21)/H(25). The AIM analysis, however, successfully did locate a BCP (20) between Rh and H(2a) on the alkyl phosphine ligand. Additional evidence for the Rh···C–C agostic interaction comes from the value of the charge density ($\rho = 0.1771$ a.u.) for BCP 1, which suggests that the C(25)–C(21) $\sigma$ bond is weakened compared with the other C–C $\sigma$ bonds [C(26)–C(21)/C(25)] of the cyclopropyl fragment [e.g., for C(25)–C(26) $\rho = 0.237$ a.u.].

**Mechanism of Binor-S′ Fluxionality.** Experimental (solution NMR) studies of **1** show that the Binor-S′ ligand has time-averaged $C_{2v}$ symmetry, indicating that a dynamic process occurs that exchanges the metallacyclobutane and cyclopropane fragments. This dynamic process has been probed by using density functional methods. For reasons of computational expediency, $[Rh(PH_3)(Binor\text{-}S')]^+$ (**4**) was used as a model for **1**. The ground-state geometry of **4** is illustrated in Fig. 2*a*, and structural parameters for this model are listed in SI Table 6. That **4** provides a suitable model for this class of rhodium complexes bearing bulkier alkyl phosphine ligands is evident through comparison with both the molecular and electronic structures of **1** and **2**. Calculated structural metrics for **4** generally are very similar to those obtained for complexes **1** and **2**. Crucially, complex **4** accurately models the interactions between rhodium and the Binor-S′ ligand, displaying two Rh–C $\sigma$ bonds [Rh–C(11)/(15) 2.029/2.029 Å] and an agostic Rh···CC interaction [Rh–C(21)/(25) 2.226/2.227 Å], with the expected lengthening of the C(21)–C(25) $\sigma$ bond (1.643 Å). Finally, to confirm the suitability of **4** as a model for complexes **1** and **2**, topological analysis of the charge density in **4** was performed by using Bader's AIM approach (58). Selected BCPs and RCPs for complex **4** are listed in SI Table 6 and shown in Fig. 2*a*. As required, characteristics of the critical points located

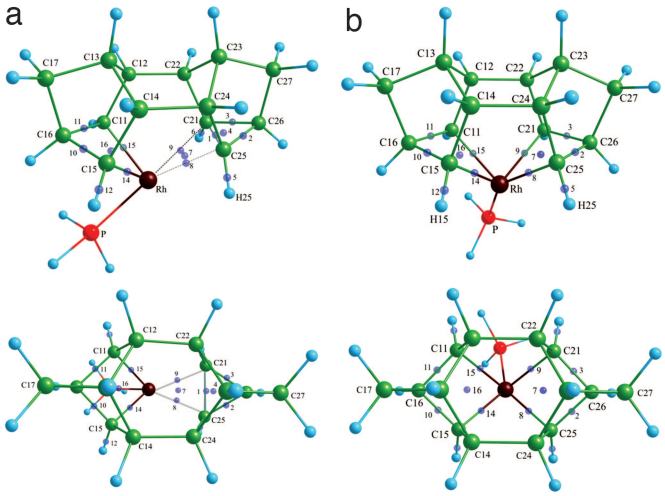


**Fig. 2.** Calculated geometries [side view (*Upper*) and projected view (*Lower*)] for **4** (*a*) and **4-Intd** (*b*). Critical points are superimposed as transparent blue spheres. Atom key: C, green; H, pale blue; Rh, brown; P, red. Selected distances (Å) and angles (°) are as follows. **4**: P–Rh–C(15) 90.1, dihedral P–Rh–C(13)–C(16) −0.4. **4-Intd**: Rh–C(21) 2.050, Rh–C(25) 2.043, Rh–C(11) 2.054, Rh–C(15) 2.063, C(11)···C(15) 2.169, P–Rh–C(15) 135.5, dihedral P–Rh–C(13)–C(16) 56.0.

in our AIM analysis of **4** are very similar to those determined for **1** and **2**. The topological features of the electron density in complex **4** indicate that this structure is unstable with respect to small changes in local structure, as would be expected for a fluxional complex. Notably, the RCP (RCP 4) for the cyclopropane fragment [C(25)–C(26)–C(21)] is nearly coincident with BCP 1 [C(25)–C(21)] (Fig. 2*a*). Similarly, RCP 7 is nearly coincident with the BCPs (8 and 9) of the Rh···C(21)–C(25) agostic interaction.

The potential energy surface of **4** was explored to elucidate possible intermediates and transition states involved in the fluxional process that exchanges the metallacyclobutane and cyclopropane fragments of the Binor-S′ ligand. This process involves movement of the phosphine from a position trans to C(21) and C(25) to one trans to C(11) and C(15). A possible intermediate (**4-Intd**) identified in our scan of the potential surface of **4** is illustrated in Fig. 2*b*, and structural parameters for **4-Intd** are listed in SI Table 6. The calculated geometry for **4-Intd** suggests that this intermediate is best described as Rh(V). The Rh–C(11)/C(15)/C(21)/C(25) distances all lie in the range 2.043–2.063 Å, which is very similar to the Rh–C bonds of the metallacyclobutane fragment in **4** [Rh–C(11)/C(15) 2.029 Å]. The C(21)–C(26)–C(25) angle for **4-Intd** (90.9°) is considerably larger than that of the ground-state complex **4** (66.3°), and the C(21)–C(25) and C(11)–C(15) separations (2.168 Å and 2.169 Å, respectively) are both outside of the normal range for a C–C bond. The plane defined by C(16)/C(13)/Rh/C(23)C(26), which bisects the C(21)–C(25) bond and the midpoint between C(11) and C(15), provides a useful point of reference from which the lateral position of the phosphine ligand can be described. In complex **4**, the $PH_3$ ligand is positioned trans to the Rh···CC agostic interaction and cis to the metallacyclobutane fragment [P–Rh–C(15) 90.1°], and it lies in the plane defined by C(16)/C(13)/Rh/C(23)C(26) [dihedral angle P–Rh–C(13)–C(16) = −0.4°]. In intermediate **4-Intd**, the P–Rh–C(15) angle is 135.5°, and the phosphine ligand lies away from the C(16)/C(13)/Rh/C(23)C(26) plane with a dihedral angle of 56.0°.

In the AIM analysis of **4-Intd** (Fig. 2*b*), four Rh–C bonds are located [Rh–C(11)/C(15)/C(21)/C(25)], and the corresponding BCPs (8, 9, 14, 15) share similar characteristics [e.g., Rh–C(25): $\rho_b$ = 0.1168; $\nabla^2\rho_b$ = 0.07272; $\varepsilon$ = 0.005], which are almost identical with those of BCPs 14 and 15 [for the Rh–C(15)/C(11) $\sigma$ bonds] in the ground state of complex **4** [e.g., Rh–C(15): $\rho_b$ = 0.1210; $\nabla^2\rho_b$ = 0.06494; $\varepsilon$ = 0.009]. The presence of four Rh–C bonds and the absence of BCPs between C(25)–C(21) and C(11)–C(15) suggests that rhodium forms two metallacyclobutane interactions with the Binor-S ligand. With the overall positive charge and the four alkyl Rh–C bonds, the oxidation state of this intermediate is described as Rh(V), in agreement with our structural analysis of **4-Intd**.

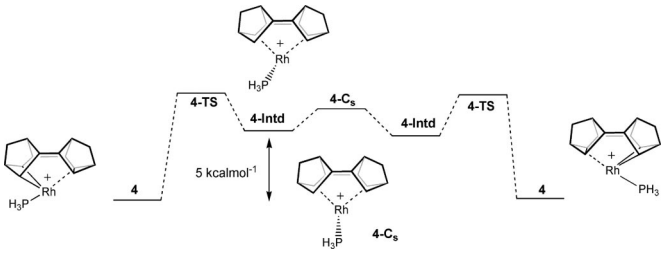


**Fig. 3.** Energy-level diagram for the structures implicated in mechanistic pathway B (Scheme 4) for the fluxional process in complex **4**.

Identification of **4-Intd** suggests pathway B (Scheme 4), which implicates a Rh(V) intermediate, is a plausible route for the fluxional mechanism that exchanges the metallacyclobutane [Rh–C(11)–C(15)] and cyclopropane [C(21)–C(26)–C(25)] fragments. Despite extensive exploration of the energy surface, we failed to locate a transition state (**4-TS**) between **4** and **4-Intd**. The lowest frequency calculated for **4-Intd** has a wave number of 19 $cm^{-1}$, suggesting the energy surface is very flat in this region. The associated motion shows movement of the $PH_3$ group toward the positions that it occupies in the equivalent ground states. We did identify a $C_s$ symmetric transition state (**4-$C_s$**) at the midpoint of the exchange, which linked **4-Intd** with its mirror image. This state had an energy 1.5 kcal·$mol^{-1}$ above **4-Intd** and an imaginary vibration of −25 *i*$cm^{-1}$, the associated motion being rotation of the phosphine.

An energy diagram for complexes **4** and **4-Intd** is provided in Fig. 3. Complex **4-Intd** is higher in energy with respect to the ground-state structure of **4** by 5.0 kcal·$mol^{-1}$. It is likely that the transition state (**4-TS**) is very similar (structurally and energetically) to **4-Intd**. The calculated energy difference between **4** and **4-Intd** compares favorably with $\Delta H^{\ddagger}$ 9.6 ± 0.2 kcal·$mol^{-1}$ obtained from our experimental measurements. It should be noted, however, that the actual pathway for the fluxional mechanism in complexes **1**, **2**, and **3** will be a more complex multistep process that additionally involves the cleavage of the Rh···CH agostic bond. Overall, our calculations suggest that the fluxional process proceeds by means of a late transition state, and the intermediates sit in shallow potential wells.

The structures of complexes **4** and **4-Intd** can be understood by considering their relation to the hypothetical structure of Binor-S coordinated to $[Rh(PH_3)]^+$. In this precursor to **4**, Rh(I) adopts a T-shaped structure in the *xy* plane, formed from two Rh···CC interactions with the intact C(21)–C(25) and C(11)–C(15) $\sigma$ bonds of the cyclopropane rings of the Binor-S ligand and the $PH_3$ ligand (positioned on the *y* axis) (Scheme 5). In complexes **1**–**3**, square-planar coordination of rhodium is completed by the agostic-H of the alkyl phosphine ligand (on the *x* axis). The *d* orbital manifold of the Rh(I) structure exhibits the expected arrangement for a square planar $d^8$ complex, with the $d_{x^2-y^2}$ orbital unoccupied (Scheme 5*a*). In the ground-state configuration of complexes **1**–**4**, back-donation from the Rh $d_{zx}$ orbital into the C(11)–C(15) bond results in oxidative addition to form a metallacyclobutane ring. The metal center has a formal oxidation state of +3, with the six *d* electrons occupying the $d_{yz}$, $d_{z^2}$, and $d_{xy}$ orbitals (Scheme 5*b*). The strong trans influence of the $PR_3$ ligand ensures that the C(21)–C(25) bond is too distant to undergo oxidative addition.

Motion of the phosphine ligand in the *xy* plane is disfavored by a repulsive interaction with the occupied $d_{xy}$, orbital. In intermediate **4-Intd**, which has been implicated in the fluxional mechanism

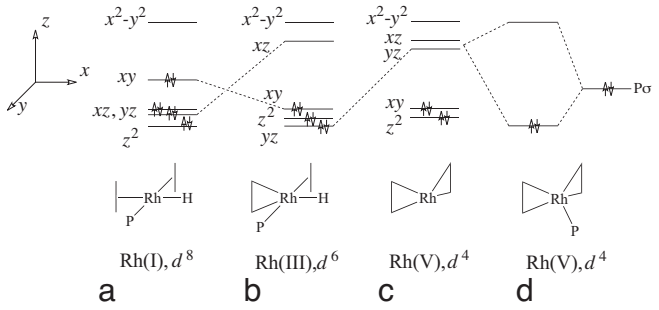


**Scheme 5.** Geometries and *d* orbital manifolds of the structures implicated in mechanistic pathway B (Scheme 4) for the fluxional process in complexes **1–3**.

that exchanges the metallacyclobutane and cyclopropane units, rhodium undergoes oxidative addition with the C(21)–C(25) bond to form a second metallacyclobutane ring. The metal center has a formal oxidation state of +5, with the four *d* electrons occupying the $d_{z^2}$ and $d_{xy}$ orbitals (Scheme 5*c*). In order for the $PR_3$ ligand to remain bound to rhodium, it coordinates either to an antibonding *d* orbital or to a linear combination *d* orbitals. From the geometry of **4-Intd**, it appears that the $PR_3$ ligand interacts with a linear combination of the $d_{xz}$ and $d_{yz}$ orbitals (Scheme 5*d*). The longer Rh–P distance in **4-Intd** (2.442 Å) compared with **4** (2.219 Å) (SI Table 7) lends support to this picture.

## Conclusions

The characterization of a M···C–C agostic bond rests on the observation of perturbations to the C–C bond on close approach to a metal center. We present here three well defined examples of complexes in which the C–C bond lengthens on interaction in the solid state, Rh–C coupling is observed in solution, and theoretical calculations clearly demonstrate a bonding interaction with the metal center. These results unequivocally point toward the presence of a $\sigma$ interaction between rhodium and the C–C single bond. There is no doubt that observation of this rare interaction is caused by the Binor-S′ ligand bringing a cyclopropane fragment in close approach to rhodium combined with the fact that the orbitals in the strained cyclopropane are energetically well set up for interaction with the metal center. That these complexes undergo reversible C–C activation in solution at room temperature, and that this can be slowed at low temperature or halted in the solid state to give $\sigma$ complexes, makes them exceptional in that they demonstrate experimentally that C–C $\sigma$ complexes are intermediates in C–C activation processes, something that has long been suggested from both indirect experimental evidence and theoretical calculations. That the pathway for C–C activation is suggested by calculations to proceed through a very rare example of a Rh(V) oxidation state only adds another facet to these intriguing complexes.

## Methods

**General Procedure for the Synthesis of Complexes 1, 2, and 3.** Under an argon atmosphere, nbd (100 $\mu$l, 930 $\mu$mol) was added to a mixture of $Na[BAr^F_4]$ (45 mg, 50 $\mu$mol) and $(PR_3)Rh(nbd)Cl$ (≈20 mg, 51 $\mu$mol) in $C_6H_5F$ (3 $cm^3$), and the solution was stirred for 2 h. The mixture was filtered, and the filtrate was layered with pentanes and held at 5°C for 48 h to give the products as yellow crystals (yields 55–82%). DFT calculations were carried out by using DFT as implemented in the ADF program suite.

**Supporting Information.** Full details of the synthesis and characterization of complexes **1–3**, NMR and crystallographic data, $^1$H variable temperature plot for **1** and computational details, including calculated geometries for complexes **1**, **2**, **4**, and **4-Intd**, can be found in SI Figs. 4 and 5, SI Data Set 1, SI Tables 2–7, and *SI Text*.

We thank Dr. Gabriele Koicok-Köhn for the collection of the data for complex **1**. We thank the Engineering and Physical Sciences Research Council (U.K.) and the Royal Society for financial support and the Oxford Supercomputing Center for support and computing facilities.

1. Rybtchinski B, Milstein D (1999) *Angew Chem Internat Ed* 38:870–883.
2. van der Boom ME, Milstein D (2003) *Chem Rev* 103:1759–1792.
3. Jun CH, Moon CW, Lee DY (2002) *Chem Eu J* 8:2423–2428.
4. Murakami M, Ito Y (1999) in *Topics in Organometallic Chemistry*, *Activation of Unreactive Bonds in Organic Synthesis*, ed Murai S (Springer, Heidelberg), Vol 3, p 97.
5. Jennings PW, Johnson LL (1994) *Chem Rev* 94:2241–2290.
6. J. Puddephatt R (1980) *Coord Chem Rev* 33:149–194.
7. Jun CH (2004) *Chem Soc Rev* 33:610–618.
8. Jun CH, Lee JH (2004) *Pure Appl Chem* 76:577–587.
9. Dyker G, ed (2005) *Handbook of C-H Transformations, Applications in Organic Synthesis* (Wiley-VCH, Weinheim, Germany).
10. Goldberg KI, Goldman AS, eds (2004) *ACS Symposium Series* (J Am Chem Soc, Washington, DC), Vol 885.
11. Simoes JAM, Beauchamp JL (1990) *Chem Rev* 90:629–688.
12. Blomberg MRA, Siegbahn PEM, Svensson M (1992) *J Am Chem Soc* 114:6095–6102.
13. Siegbahn PEM, Blomberg MRA (1992) *J Am Chem Soc* 114:10548–10556.
14. Diggle RA, Macgregor SA, Whittlesey MK (2004) *Organometallics* 23:1857–1865.
15. Jazzar RFR, Macgregor SA, Mahon MF, Richards SP, Whittlesey MK (2002) *J Am Chem Soc* 124:4944–4945.
16. Perthuisot C, Edelbach BL, Zubris DL, Simhai N, Iverson CN, Muller C, Satoh T, Jones WD (2002) *J Mol Cat* 189:157–168.
17. Kubas GJ (2001) *Metal Dihydrogen and σ-Bond Complexes* (Kluwer/Plenum, New York).
18. Labinger JA, Bercaw JE (2002) *Nature* 417:507–514.
19. Suresh CH, Koga N (2004) *Organometallics* 23:76–80.
20. Jones WD (2003) *Acc Chem Res* 36:140–146.
21. Clot E, Eisenstein O (2004) in *Principles and Applications of Density in Inorganic Chemistry II*, Vol 113, pp 1–36.
22. Shilov AE, Shul'pin GB (2000) *Activation and Catalytic Reactions of Saturated Hydrocarbons in the Presence of Metal Complexes* (Kluwer, Dordrecht, The Netherlands).
23. Periana RA, Bergman RG (1986) *J Am Chem Soc* 108:7346–7355.
24. Wick DD, Northcutt TO, Lachicotte RJ, Jones WD (1998) *Organometallics* 17:4484–4492.
25. Rodriguez-Garcia C, Oliva A, Ortuno RM, Branchadell V (2001) *J Am Chem Soc* 123:6157–6163.
26. Hill GS, Puddephatt RJ (1998) *Organometallics* 17:1478–1486.
27. Georgii IN (2003) *Angew Chem Internat Ed* 42:1335–1337.
28. Chen W, Shimada S, Tanaka M (2002) *Science* 295:308–310.
29. Goldfuss B, von Ragué Schleyer P, Hampel F (1996) *J Am Chem Soc* 118:12183–12189.
30. Tomaszewski R, Hyla-Kryspin I, Mayne CL, Arif AM, Gleiter R, Ernst RD (1998) *J Am Chem Soc* 120:2959–2960.
31. Harvey BG, Mayne CL, Arif AM, Tomaszewski R, Ernst RD (2006) *J Am Chem Soc* 128:1770 (Correction).
32. Bader RFW, Matta CF (2001) *Inorg Chem* 40:5603–5611.
33. Vigalok A, Rybtchinski B, Shimon LJW, Ben-David Y, Milstein D (1999) *Organometallics* 18:895–905.
34. Gandelman M, Konstantinovski L, Rozenberg H, Milstein D (2003) *Chem Eu J* 9:2595–2602.
35. Frech CM, Milstein D (2006) *J Am Chem Soc* 128:12434–12435.
36. Jaffart J, Cole ML, Etienne M, Reinhold M, McGrady JE, Maseras F (2003) *Dalton Trans*, 4057–4064.
37. Jaffart J, Etienne M, Reinhold M, McGrady JE, Maseras F (2003) *J Chem Soc Chem Commun*, 876–877.
38. Maseras F, Crabtree RH (2004) *Inorg Chim Acta* 357:345–346.
39. Suresh CH, Baik MH (2005) *Dalton Trans*, 2982–2984.
40. Gandelman M, Shimon LJW, Milstein D (2003) *Chem Eu J* 9:4295–4300.
41. Gandelman M, Vigalok A, Konstantinovski L, Milstein D (2000) *J Am Chem Soc* 122:9848–9849.
42. Brookhat M, Green MLH (1983) *J Organomet Chem* 250:395–408.
43. Brookhart M, Green MLH, Wong LL (1988) *Prog Inorg Chem* 36:1–124.
44. Ingleson MJ, Mahon MF, Weller AS (2004) *Chem Commun*, 2388–2389.
45. Brayshaw SK, Green JC, Kociok-Kohn G, Sceats EL, Weller AS (2006) *Angew Chem Internat Ed* 45:452–456.
46. Schrock RR, Osborn JA (1971) *J Am Chem Soc* 93:3089–3090.
47. Boer FP, Neuman MA, Roth RJ, Katz TJ (1971) *J Am Chem Soc* 93:4436–4442.
48. Baratta W, Mealli C, Herdtweck E, Ienco A, Mason SA, Rigo P (2004) *J Am Chem Soc* 126:5549–5562.
49. Braga D, Grepioni F, Biradha K, Desiraju GR (1996) *J Chem Soc Dalton Trans*, 3925–3930.
50. D'Accolti L, Fusco C, Lucchini V, Carpenter GB, Curci R (2001) *J Org Chem* 66:9063–9066.
51. Webster CE, Hall MB (2001) *Organometallics* 20:5606–5613.
52. Cotton FA, Wilkinson G (1998) *Advanced Inorganic Chemistry* (Wiley, New York).
53. *gNMR* (Adept Scientific, Herts, UK), Version IV.
54. Karshtedt D, Bell AT, Tilley TD (2006) *Organometallics* 25:4471–4482.
55. Fernandez MJ, Bailey PM, Bentz PO, Ricci JS, Koetzle TF, Maitlis PM (1984) *J Am Chem Soc* 106:5458–5463.
56. Duckett SB, Haddleton DM, Jackson SA, Perutz RN, Poliakoff M, Upmacis RK (1988) *Organometallics* 7:1526–1532.
57. Brunkan NM, Brestensky DM, Jones WD (2004) *J Am Chem Soc* 126:3627–3641.
58. Bader RFW (1994) *Atoms in Molecules*: *A Quantum Theory* (Oxford Univ Press, New York).
59. Bader RFW (1991) *Chem Rev* 91:893–928.